

Resonance Raman scattering studies in Br₂-adsorbed double-wall carbon nanotubes

A. G. Souza Filho,^{1,*} M. Endo,² H. Muramatsu,² T. Hayashi,² Y. A. Kim,² E. B. Barros,^{1,6} N. Akuzawa,³ Ge. G. Samsonidze,⁵ R. Saito,⁴ and M. S. Dresselhaus^{5,6}

¹*Departamento de Física, Universidade Federal do Ceará, 60455-900 Fortaleza, Ceará, Brazil*

²*Faculty of Engineering, Shinshu University, 4-17-1 Wakasato, Nagano-shi 380-8553, Japan*

³*Tokyo National College of Technology, 1220-2 Kunugida-machi, Hachioji-shi, Tokyo 193-0997, Japan*

⁴*Department of Physics, Tohoku University, and CREST, JST, Sendai 980-8578, Japan*

⁵*Department of Electrical Engineering and Computer Science, Massachusetts Institute of Technology, Cambridge, Massachusetts 02139-4307, USA*

⁶*Department of Physics, Massachusetts Institute of Technology, Cambridge, Massachusetts 02139-4307, USA*

(Received 11 January 2006; revised manuscript received 19 April 2006; published 16 June 2006)

The vibrational and electronic properties of Br₂-adsorbed double-wall carbon nanotubes (DWNTs) were investigated by resonance Raman scattering. Special attention was given to distinguish the behavior between S/M and M/S outer/inner semiconducting (S) and metallic (M) tubes. By using three laser excitation energies 2.33, 1.96, and 1.58 eV, resonance Raman spectra were obtained for the DWNTs before and after bromine adsorption, and also for the Br-Br molecular resonance, thereby facilitating the study of charge transfer between the DWNTs and the bromine. It was found that Br₂ molecules act as acceptors and that metallic nanotubes are specially sensitive to the presence of Br₂ molecules even when they constitute the inner tubes of DWNTs.

DOI: [10.1103/PhysRevB.73.235413](https://doi.org/10.1103/PhysRevB.73.235413)

PACS number(s): 73.22.-f, 78.30.Na

I. INTRODUCTION

Carbon nanotubes are nanostructured materials which exhibit striking properties regarding their geometrical and electronic structure. Most studies of carbon nanotube systems are performed on single-walled (SWNT) and multiwalled (MWNT) nanotubes. However, there has recently been an increase of interest in double-walled carbon nanotubes (DWNTs). The DWNT system is interesting in its own right because it is an intermediate structure between SWNTs and MWNTs. DWNTs have only two tubes and the diameters of the outer tubes are often similar to those of SWNTs. The quantum confinement effects for the inner tubes are very prominent due to their small diameters. Furthermore, DWNTs are structurally more stable than SWNTs. Recent advances in synthesis have allowed the production of very high quality DWNTs with a very small amount of SWNT constituents.¹ This DWNT system should be useful for cylindrical molecular capacitors, GHz oscillators, nanocomposites, field emission sources, nanotube bicables, electronic devices, and other applications.¹⁻⁴

The control/tuning of the electronic properties of nanotubes is a key point for transforming their potential into real-world technology. One way for achieving this control/tuning is by carrying out donor or acceptor doping experiments where either electrons or holes are added to the carbon nanotube through intercalation and/or functionalization processes.⁵⁻¹⁰ By doping nanotubes in a controlled way, it is possible to assess how specific chemical species perturb their electronic properties. In addition, these modified systems also open up the opportunity for studying the basic physical properties of nanotubes in a controlled way.

The intercalation of carbon nanotubes with electron donors and electron acceptors is now a very active research field and many efforts have been directed toward understand-

ing and controlling the electronic properties of SWNTs, DWNTs, and MWNTs.^{6,11-13} In particular, the effects of the Br₂ interaction with carbon nanotubes have been reported for SWNTs (Ref. 5) and more recently for DWNTs.² Rao *et al.*⁵ have claimed very large Raman frequency upshifts in both the RBM and *G* band for brominated SWNTs, thus indicating a strong acceptor behavior for Br₂ molecules. Chen *et al.*² have assumed that 90% of the charge is located in the outer tube. By using the equation $\Delta\omega$ (cm⁻¹) = 460*f* (where *f* is the charge transfer) for estimating the charge transfer, they correlate their observed 16 cm⁻¹ upshift of the *G* band for the outer tubes to correspond to creating 1/26 holes per carbon atom. This amount of charge induces a Fermi level depression of 1.2–1.4 eV as a result of their level of bromination.²

The Raman spectra of most graphite intercalation compounds only exhibit peaks from the graphite host and only for a few dopants is it possible to observe the spectra of the intercalant species.¹⁴ The graphite-Br₂ intercalation compounds are an especially interesting system because this system allows the observation of the Raman spectra from both the host carbon and from the guest Br₂ species.¹⁴

In this paper we report a study of Br₂ adsorbed by high purity bundled DWNTs (essentially free of catalyst particles and SWNTs) using resonance Raman scattering as a probe. In Br₂-doped DWNTs we observed the resonance Raman spectra of both the DWNTs and the Br₂ thus allowing us to get additional insights when studying the charge transfer between the dopant and the host DWNTs. The use of different laser lines allowed us to study different configurations of outer/inner tubes separately, such as M/S and S/M outer/inner metallic (M) and semiconducting (S) DWNTs, and to contrast the difference in screening effects for these two cases. The inner tubes have a small diameter, thus allowing us to study the effects of doping on the $2n+m$ families and to

identify the specific (n, m) tubes that are resonant in each spectrum. Both decreases and increases in the radial breathing mode (RBM) intensity due to bromination are observed and accounted for. We have also observed the resonance spectra from DWNTs for which E_{laser} is in resonance with $E_{11}^{\text{M}}(\text{H})$, the higher energy van Hove singularity for metallic nanotubes, a virtually unexplored phenomenon.¹⁵ The S/S configuration was also studied and our results for this configuration differ from those previously reported,² the differences most likely coming from the different amounts of charge transfer due to different dopant levels. Furthermore, we have found that Br_2 molecules interact with the DWNTs, and their intercalation and de-intercalation are completely reversible upon thermal annealing at 600 °C. Upshifts in the Raman frequencies for the tangential G^+ modes and depression of their Raman intensities indicated that electrons are transferred from the nanotubes to the Br_2 molecules. Metallic nanotubes are specially sensitive to the adsorption of Br_2 molecules, even when they are the inner tubes of DWNTs.

II. EXPERIMENT

The synthesis of DWNTs was carried out by a catalytic chemical vapor deposition (CCVD) method utilizing a conditioning catalyst ($\text{Mo}/\text{Al}_2\text{O}_3$) at one end of the furnace, and a nanotube growth catalyst (Fe/MgO) placed in the middle part of the furnace.¹ Subsequently, a $\text{CH}_4 + \text{Ar}$ (1:1) mixture was fed into the reactor, typically for 10 min at 875 °C. In order to obtain a highly pure DWNT web, a two-step purification process was applied to the synthesized products. In particular, a hydrochloric acid (18% concentration, at 100 °C for 10 h) treatment was carried out in order to remove the MgO and iron catalyst particles, followed by air oxidation at 500 °C for 30 min. Then we prepared a highly dispersed solution containing DWNTs (15 mg in 100 ml ethanol) using ultrasonication (KUBOTA UP50H) for 30 min, without any surfactant. By filtering a stable suspension of DWNTs [polytetrafluoroethylene (PTFE) filter, 1 μm], drying the filtered material for 24 h in vacuum and peeling off the resulting bucky paper from the PTFE filter very carefully, we finally obtained a black DWNT bucky paper sample which is thin, flexible and tough enough mechanically to fold in origami. This DWNT bucky paper was used for the pristine undoped comparison sample. The magnetic characterization of the sample indicates a diamagnetic behavior, thus confirming the absence of metallic catalyst particles dispersed into the bundles.¹

The brominated sample was prepared from the DWNT bucky paper by the following procedure. The bromination of the DWNT bucky paper was performed by reacting the DWNTs with Br_2 vapor for 5 days at room temperature. We thus obtained highly stabilized brominated DWNTs that were stable in an air atmosphere. The stoichiometry of the brominated DWNT sample used in these experiments was C_{21}Br .

The Raman experiments were performed at room temperature using a Kaiser HoloLab5000 system for $E_{\text{laser}} = 2.33$ eV (532 nm) excitation and a Horiba-Jobin Yvon setup for $E_{\text{laser}} = 1.96$ eV (633 nm) and $E_{\text{laser}} = 1.58$ eV (785 nm) excitations.

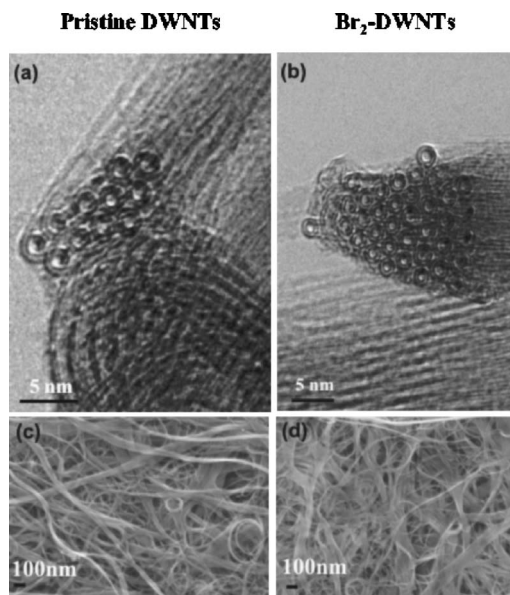


FIG. 1. Transmission electron microscope (TEM) images of pristine double-wall carbon nanotubes (a) before and (b) after Br_2 adsorption. (c) and (d) show, respectively, scanning electron microscope (SEM) images, for both pristine and Br_2 -doped DWNTs.

III. RESULTS AND DISCUSSION

A. Sample characterization

Figures 1(a) and 1(b) show high-resolution TEM images of pristine and Br_2 -adsorbed DWNTs. It is clear from the TEM images and other sample characterizations⁴ that the samples are of very high quality (99% of DWNTs and 1% of SWNTs+catalyst particles). Very large areas were probed with SEM [see panels (c) and (d)] and these images did not reveal the presence of any metal particles or amorphous carbon. The diameter distribution of both the inner ($d_i = 0.86 \pm 0.25$ nm) and outer ($d_o = 1.56 \pm 0.31$ nm) tubes were determined from TEM images. We did not observe any structural or morphological changes between the pristine and Br_2 -adsorbed DWNTs from the TEM and SEM images. This result indicates that the Br_2 molecules are not intercalating between the inner and outer tubes within DWNTs, a result that is also supported by the Raman results described below.

B. Radial breathing mode spectra vs electronic transitions

The DWNT system allows one to probe different configurations of the outer and inner tubes. Depending on the laser energy used for exciting the spectra, it is possible to have both outer and inner tubes in resonance with a given laser line. Depending on the diameter distribution, it is possible to have outer/inner configurations as follows: S/M, M/S, S/S, and M/M (S and M denote semiconducting and metallic nanotubes, respectively). Since the inner tubes have small diameter values, their electronic transition energies are well separated from each other, thus allowing one to correlate selected radial breathing mode (RBM) frequencies observed in the Raman spectra with specific (n, m) values.

The resonance Raman scattering results can be discussed in detail by examining the diameter dependent electronic

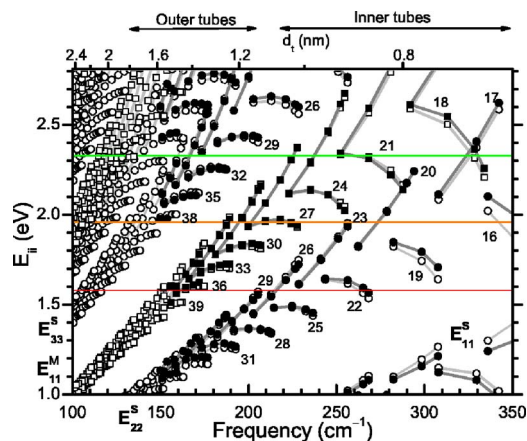


FIG. 2. (Color online) Calculated E_{ii} values for semiconducting (S) (open circles) and metallic (M) (open squares) tubes vs radial breathing mode frequency ω_{RBM} (bottom horizontal axis) and nanotube diameter (top horizontal axis). The open and solid symbols, respectively, stand for pristine and for 0.04 electron/carbon atom deficient bromine doped nanotubes (Refs. 18 and 21). The three horizontal lines stand for the 1.58, 1.96, and 2.33 eV laser energies used for excitation of the Raman spectra. The family behavior is indicated by the $2n+m$ values for the E_{22}^S and E_{11}^M transitions (see text). We indicate in the upper part of the figure the frequency domain where the main contributions of the inner and outer tubes to the RBM spectra are expected based on the diameter distribution of the sample and the spectrometer limitations at low wave numbers. The calculations for doped tubes were performed only for the diameter range compatible with our samples.

properties of single wall carbon nanotubes. In Fig. 2 we show the so-called Kataura plot which is a plot of electronic transition energies as a function of the radial breathing mode frequency ω_{RBM} , where ω_{RBM} is related to the tube diameter by $\omega_{\text{RBM}} = A/d_t + B + (C + D \cos 3\theta)/d_t^2$, with ω_{RBM} and d_t in units of cm^{-1} and nm, respectively.¹⁶ The A , B , C , and D values used for constructing this plot were, respectively, 223 (228), 73 (14), -1.1 (-2.7), and -0.9 (-2.7) for semiconducting (metallic) nanotubes.

The electronic transition energies (E_{ii}) for different (n, m) nanotubes are calculated from the extended tight-binding model (ETB) that takes into account rehybridization of σ and π orbitals induced by the curvature of the SWNT sidewall and long-range atomic interactions beyond the first nearest-neighbor in the graphene sheet.^{17,18} This model successfully accounts for the family patterns observed in the photoluminescence emission data.¹⁹ The geometrical structure relaxation is performed by minimizing the total energy of the SWNT calculated from the ETB model, which is essential for establishing a proper family behavior for the E_{ii} energies in the small diameter (large ω_{RBM}) region of the Kataura plot.¹⁶ An almost rigid blueshift by 0.2–0.3 eV is then applied to the calculated E_{ii} family lines to account for the many-body effects (quasiparticle corrections and exciton binding energies) to account for the empirical corrections proposed by Jorio *et al.*¹⁶ The resulting E_{ii} energies are shown in Fig. 2 by open symbols. We then remove 1% of the electrons from the SWNTs (0.04 electron per carbon atom deficient doping) and perform a geometrical structure relax-

ation once again, consequently calculating the E_{ii} energies based on the ETB model. The same many-body corrections are then applied to the ground state E_{ii} energies as in the case of pristine SWNTs.¹⁶ Even though the many-body corrections are expected to change with electron doping, we do not have sufficient experimental data to establish this dependence following the fitting procedure developed in Ref. 16. Anyway, the many-body corrections contribute only a small fraction of the ground state E_{ii} energy, and thus their dependence on electron doping is not expected to change the optical transition E_{ii} energy for any (n, m) tube to a first approximation.

We should comment here that the terminology we are using in this paper is that for resonance of the laser excitation with band to band transitions between so called van Hove singularities. However, the reader should be aware that the mechanism involved in observed optical phenomena is better described by considering an excitonic picture, involving bright exciton transitions rather than band to band transitions. The plot shown in Fig. 2 and evaluated by the ETB model is also valid for the optically allowed bright excitonic transitions. Therefore, the formalism previously used for transitions between van Hove singularity is also applicable for the excitonic picture by using the ETB model after including many-body corrections.

The horizontal lines in Fig. 2 correspond to the excitation laser energies 1.58, 1.96, and 2.33 eV used in the present work. The open and solid symbols, respectively, denote the electronic transitions for undoped and doped nanotubes (0.04 electron/carbon atom being removed from the nanotubes as a result of doping). The nanotube families observed in the plot of Fig. 2 are characterized by $2n+m=p$ (the numbers p are given in the figure), where n and m are integers defining the carbon nanotube structure for individual (n, m) tubes. For metallic SWNTs, it is necessary to consider the trigonal warping effect and its consequence on the electronic properties. Depending on the tube chirality, this effect causes a splitting of each van Hove singularity for metallic nanotubes into lower [$E_{ii}^M(L)$] and higher [$E_{ii}^M(H)$] energy components. This effect causes each $2n+m$ family for metallic nanotubes to exhibit a lower and an upper energy branch. The common point of the upper and lower energy branches is the armchair (n, n) nanotube. The magnitude of the $E_{ii}^M(H) - E_{ii}^M(L)$ splitting varies from zero for armchair nanotubes (n, n) (the central member of each family in the metallic E_{11}^M sub-band) to a maximum splitting for both metallic $(3n, 0)$ zig-zag and $(3n+1, 1)$ nanotubes (the end members for each family of a metallic subband), where n is an integer.²⁰ By examining this plot, we can easily identify the outer/inner tube configurations that will be resonant for a given excitation energy, and whether the tubes in resonance are semiconducting or metallic. Of particular interest in the present work is the study of individual $2n+m=p$ families as bromine doping takes place.

1. Semiconducting outer/metallic inner tube configuration

Figure 3 shows the Raman spectra of the radial breathing modes (RBMs) taken with $E_{\text{laser}} = 2.33$ eV for both pristine and Br₂-adsorbed DWNTs. The RBM spectrum of pristine DWNTs clearly shows the presence of two groups of ω_{RBM}

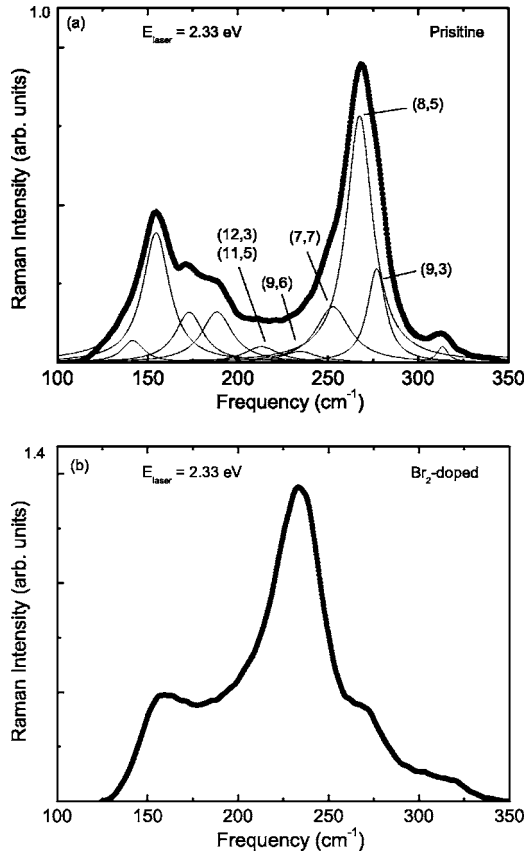


FIG. 3. Raman spectra taken with $E_{\text{laser}}=2.33 \text{ eV}$ for pristine (a) and Br_2 -adsorbed (b) DWNTs in the RBM spectral region.

frequencies that are related to the inner (higher frequency) and outer (lower frequency) tubes with the S/M configuration dominating. According to the electronic transition energies between van Hove singularities (see Fig. 2), $E_{\text{laser}}=2.33 \text{ eV}$ is in resonance with E_{11}^M (E_{33}^S and E_{44}^S) for the inner (outer) tubes, which are metallic (semiconducting).^{2,6} However, due to the notch filter cutoff, we observe in the RBM spectra only those tubes that are resonant with E_{33}^S .

First, we look at the origin of the large intensity peaks in Fig. 3. The strongest peak located near 270 cm^{-1} is associated with metallic tubes belonging to the $2n+m=21$ family and resonant with $E_{11}^M(L)$ transitions (lower energy branch). This strong peak is identified as having contributions coming mainly from three nanotubes, given in order of decreasing diameter or increasing ω_{RBM} frequencies as the (7,7), (8,5), and (9,3) tubes, and the line shape analysis shows that they correspond, respectively, to the observed RBM peak frequencies of 253 , 267 , and 277 cm^{-1} . Both the (7,7) and (8,5) tubes are in a very good resonance condition, insofar as their transition energies are very close to the laser energy 2.33 eV (see Fig. 2). However, the intensity is also dependent on matrix elements, and armchair nanotubes, because of their smaller predicted matrix elements, are expected to have a lower intensity than the other tubes within the same $2n+m$ family.²² Thus the highest intensity peak was assigned to the (8,5) nanotube for $E_{\text{laser}}=2.33 \text{ eV}$ in resonance with the $E_{11}^M(L)$ transition energy. The (9,3) tube on the $E_{11}^M(L)$ transi-

tion branch is not close to the laser energy and therefore a low intensity is expected for this RBM feature.

Another group of frequencies that contribute strongly to the RBM spectra at $E_{\text{laser}}=2.33 \text{ eV}$ are observed from 150 to 200 cm^{-1} and these peaks are due to the outer tubes. By examining the plot in Fig. 2, we can see that many tubes, predominantly semiconducting tubes, can contribute to a Raman signal near the frequency of 150 cm^{-1} . However, for the peaks close to 200 cm^{-1} we can identify that the observed RBM features come from family 32, and perhaps also from family 29 where $E_{\text{laser}}=2.33 \text{ eV}$ is weakly resonant with E_{33}^S transitions.

It is interesting to note that the 2.33 eV laser energy is also very close to two members of the 27 and 24 families which would be expected to yield a high intensity for those tubes if we consider only the $E_{\text{laser}} \approx E_{11}^M$ resonance condition. However, the intensity of the peaks observed at 235 and 241 cm^{-1} are very weak and this is related to the fact that those resonant E_{ii} values belong to the higher energy branch for metallic tubes [$E_{11}^M(H)$] which is predicted by theory to have a low Raman intensity, in part because of their weaker matrix elements.²³ Indeed, the observation of this resonance was not previously reported for studies on isolated SWNTs by using tunable lasers.²⁴ Similar evidence for the observation of an RBM signal in resonance with $E_{11}^M(H)$ transitions for metallic tubes has also been observed recently for SWNTs on a Si/SiO₂ substrate.¹⁵

We now comment on the weak peak observed at 313 cm^{-1} for pristine DWNTs in Fig. 3(a). By examining the Kataura plot, it is not expected that any RBM frequency near 313 cm^{-1} would be in resonance with 2.33 eV . The closest (n,m) tube that would be in resonance is the (8,2) tube (family 18), but the expected frequency for this tube is 321 cm^{-1} which is upshifted by 8 cm^{-1} from 313 cm^{-1} . Therefore, the peak at 313 cm^{-1} is not clearly identified yet and we would need more laser lines for establishing its (n,m) identity and its resonant behavior.

We now analyze the Br_2 doping effect on the RBM spectra measured with $E_{\text{laser}}=2.33 \text{ eV}$ whose spectrum is shown in Fig. 3(b). We note that the peaks attributed to metallic inner tubes (7,7), (8,5), and (9,3) in the pristine sample (family 21) likely decrease in intensity relative to the outer semiconducting nanotubes upon doping. In Fig. 2 (solid circles), we show the electronic transition energies of nanotubes when they have a deficiency of 0.04 electron/carbon. We can observe that Br_2 doping affects the electronic transition energies of nanotubes, depending on both their diameter and chiral angle. We can see that bromine doping is predicted to lower the $E_{11}^M(L)$ transition energies of family 21 for the Br_2 doped nanotubes only slightly, consistent with their observed intensity decrease.

The strong mode in Fig. 3(b) peaked at about 232 cm^{-1} is assigned to the Br-Br stretching mode of the Br_2 molecule which we will discuss separately in Sec. III C.¹⁴ The peak from the Br-Br mode is very strong, thus making the line shape analysis for the RBM features from the nanotubes imprecise. Thus, for the Br_2 -doped DWNTs in the low ω_{RBM} frequency region, we do obtain information about Br-Br bonds (see Sec. III D), but we do not obtain that much de-

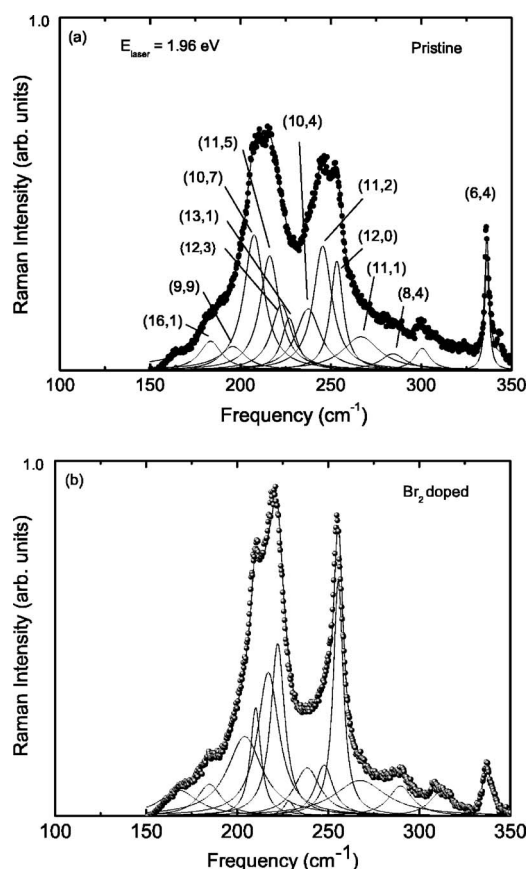


FIG. 4. Raman spectra taken with $E_{\text{laser}}=1.96$ eV for pristine (a) and Br₂-adsorbed (b) DWNTs in the RBM spectral region.

tailed information on the effect of bromine doping on the nanotube RBM features in Fig. 3(b). However, the effect of the Br₂ doping on the RBM spectra can be analyzed by exciting the Raman spectra with other laser lines which are not in resonance with electronic transitions for the Br₂ system, as we discuss in the next two subsections.

2. Probing only inner tubes

The RBM Raman spectrum obtained with $E_{\text{laser}}=1.96$ eV for pristine DWNTs is shown in Fig. 4(a). Since the outer tubes in our sample and spectra window are not resonant (see Fig. 2) with this laser line, we conclude that the RBM spectra in Fig. 4 are associated mainly with inner tubes (both metallic and semiconducting). From 180 to 250 cm⁻¹ the contribution to the spectra in Fig. 4(a) comes from metallic inner tubes, but the strong highest frequency peak at 336 cm⁻¹ comes from a semiconducting nanotube. This isolated peak at 336 cm⁻¹ is assigned to the (6,4) tube. We note that the (6,4) peak for the pristine DWNT is very sharp, thus confirming its weak interaction with its outer semiconducting tube. In the 180–250 cm⁻¹ range, where the large intensity RBM features are found, we can attribute the observed spectra mainly to tubes that are members of families 27 and 24 for metallic tubes. The members associated with family 27 are, in order of increasing frequency, (9,9), (10,7), (11,5), (12,3), and (13,1). By examining Fig. 2, we can see that 1.96 eV would be resonant with other metallic nanotubes

that would contribute with frequencies below 200 cm⁻¹. The end members of family 24 are, in order of increasing RBM frequency, (10,4), (11,2), and (12,0). The RBM frequencies observed for these pristine tubes in Fig. 4(a) are 243, 248, and 252 cm⁻¹. The transition energies of (11,2) and (12,0) are close to E_{laser} and they appear in the spectra with strong intensity. Again, we point out the low intensity (or absence) of features related to resonance with the higher energy transition in metallic nanotubes [$E_{11}^M(H)$] (for families 30 and 33) is due to the small magnitude of their matrix elements.²² We could only see weak peaks at 168 and 186 cm⁻¹ which can be assigned to the (16,1) and (9,9) nanotubes in resonance with E_{11}^M . Although these features are weak, we have again seen evidence at $E_{\text{laser}}=1.96$ eV for the observation of RBM peaks in the Raman spectra resonant with the higher energy $E_{11}^M(H)$ transitions for metallic nanotubes in DWNTs.

We now analyze the effect of Br₂ doping on the RBM spectra obtained with 1.96 eV laser excitation energy. First, we should point out that at $E_{\text{laser}}=1.96$ eV we did not observe the Raman spectra at 232 cm⁻¹ from the Br₂ molecule, as we did for the 2.33 eV laser excitation energy. We attribute the absence of the Br-Br mode in Fig. 4(b) to the observation that the electronic resonance window corresponding to this Br-Br vibration is sharp and close to 2.33 eV. We can see by comparing Figs. 4(a) and 4(b) that the RBM spectral intensity for both the semiconducting and metallic inner tubes are affected by the Br₂ doping. The bromine doping affects these intensities in two ways. There is a considerable enhancement of the intensity of certain RBM modes below 250 cm⁻¹ and a considerable depression of the RBM mode at 336 cm⁻¹, as discussed below.

The enhancement of the modes located between 200 and 250 cm⁻¹ can be understood by considering the changes in the electronic transition energies induced by doping, which Fig. 2 shows to generally enhance the resonance process. We can observe that the end members of family 27 [(12,3), (13,1)] increase their energy $E_{11}^M(L)$ by a few meV, thus bringing these tubes into better resonance and thus increasing the intensity of these features upon bromine doping. Figure 2 shows that the end members of family 24 [(11,2) and (12,0)] decrease their electronic transition energies upon bromination, thus allowing the transition energies for these tubes to get closer to $E_{\text{laser}}=1.96$ eV, and for this reason we also predict an enhancement in their intensities as we can experimentally observe in Fig. 4(b). The relative enhancement is observed to be higher for the higher frequency modes of the 27 and 24 families, which is also consistent with the fact that, after doping, those tubes are the ones that get closer to the laser energy than the others. The lineshape analysis shows that the observed shift in the RBM frequencies is very small for the metallic inner tubes upon doping. A more detailed study with more laser lines is needed to measure any small frequency shifts that might occur.

Bromination causes the intensity (linewidth) of the (6,4) peak to decrease (increase). This result indicates a weakening in the resonant process by bromination. For the pristine sample, the E_{22}^S energy is close to $E_{\text{laser}}=1.96$ eV but after bromination, the predicted E_{22}^S transition energy is upshifted by 80 meV for 0.04 electron/carbon atom transfer from the

nanotube to the adsorbed bromine (solid circle in Fig. 2). The experimental upshift of E_{22}^S in energy for the (6,4) tube is enough to bring the (6,4) tube into a relatively weak resonance condition. The relevant point is that E_{22}^S will upshift to a less favorable resonant condition for this tube upon Br_2 doping, in agreement with the experimental observation.

The (6,4) tube diameter is 0.68 nm. By considering that the inner-outer shell distance is about 0.35 nm, we can estimate the diameter of the outer shell and determine if it is metallic or semiconducting. The outer tube diameter is thus expected to be $\sim 0.68 + 2 \times 0.35 = 1.38$ nm, which converting to ω_{RBM} would lead to a nanotube with a RBM frequency of around 160 cm^{-1} . By examining the Kataura plot in Fig. 2, we see that the outer shell for the (6,4) tube can be a semiconducting or a metallic tube, and thus we are also probing the S/S DWNT configuration with this tube. No shift in the peak frequency 336 cm^{-1} associated with the RBM of the (6,4) tube is observed upon bromination, thus indicating that semiconducting inner tubes are not very much affected by bromine doping when the outer tube is semiconducting. A similar result for semiconducting inner tubes is obtained when the outer tube is metallic as we discuss next for the M/S configuration.

3. Metallic outer/semiconducting inner configuration

We also have analyzed the RBM Raman spectra of pristine and Br_2 -adsorbed DWNTs by exciting the spectra with $E_{\text{laser}} = 1.58 \text{ eV}$. The results are shown in Figs. 5(a) and 5(b). According to Fig. 2 it is expected that the spectra excited with $E_{\text{laser}} = 1.58 \text{ eV}$ will be in resonance with semiconducting inner and metallic outer tubes. The spectrum reported here for $E_{\text{laser}} = 1.58 \text{ eV}$ is resonant with the E_{11}^M and E_{22}^S electronic transitions for the DWNT sample under investigation. Some tubes can be also in resonance with E_{33}^S but their RBMs are not located in the frequency region shown in Fig. 5.

We first analyze the resonance of $E_{\text{laser}} = 1.58 \text{ eV}$ with the E_{22}^S electronic transitions for the inner tubes in a M/S configuration. The strong features around 270 cm^{-1} in Fig. 5(a) are identified as coming from the response of the three end members of the $2n+m=22$ family (semiconducting nanotubes) which are, in increasing order of RBM frequencies assigned to the (9,4), (10,2), and (11,0) tubes, with frequencies at 264, 268, and 274 cm^{-1} , respectively, for the pristine sample. The end members are expected to have large electron-phonon coupling matrix elements and thus are expected to have large Raman intensities.²³

The Raman peaks from metallic outer tubes ($E_{\text{laser}} = 1.58 \text{ eV}$ in resonance with E_{11}^M) are weak in part because of the cut-off condition of the notch filter used in our experiments. In the case of Br_2 -doped samples, their weak intensity also provides evidence for a depletion of the electronic states due to doping. We will discuss this issue when analyzing the G-band spectra in Sec. III C. However, by analyzing the intensities shown in Fig. 5(a), we can state that the weak band observed from 150 to 170 cm^{-1} is due to the resonance of $E_{\text{laser}} = 1.58 \text{ eV}$ with E_{22}^S for members of family 39. Since the diameters are large, the RBM frequencies for the different (n,m) are very close to each other and they overlap with

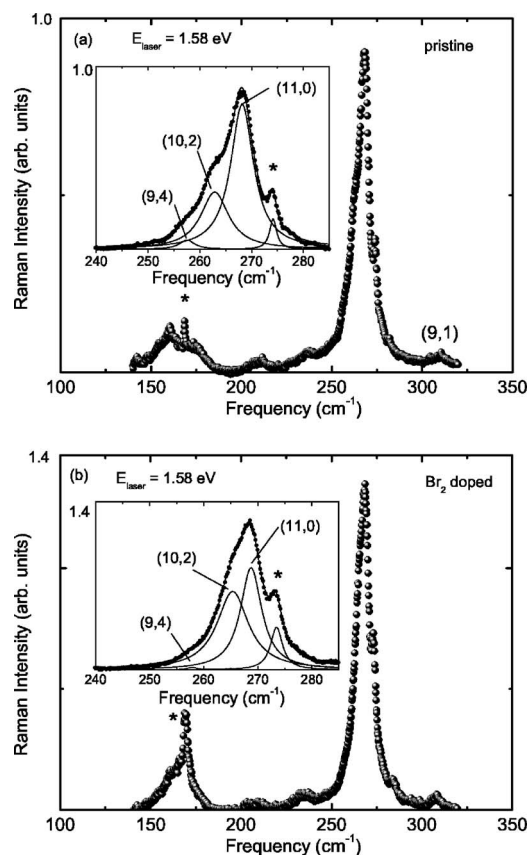


FIG. 5. Raman spectra taken with $E_{\text{laser}} = 1.58 \text{ eV}$ for pristine (a) and Br_2 -adsorbed (b) DWNTs in the RBM spectral region. The sharp peaks near 170 and 272 cm^{-1} marked with an asterisk are experimental artifacts. The inserts show the lineshape analyses for the spectral region of 250 – 280 cm^{-1} .

each other, thus not allowing individual tubes to be clearly resolved in the experimental spectrum. The weak peak near 310 cm^{-1} can however be attributed to the (9,1) nanotube of family $2n+m=19$. Other weak features close to 211 and 236 cm^{-1} can be identified as coming from the members of the semiconducting 29 and 26 families. These features are weak because the (14,1) end member of family 29, the (12,2) second member of family 26, and the (11,1) first member of family 23 all have weak matrix elements which account for their low intensity.²²

The changes in the RBM features after bromination for 1.58 eV are not so large as they are for $E_{\text{laser}} = 2.33$ and 1.96 eV . We can observe that in the RBM spectral region, the outer tubes in Fig. 5(b) experience changes in their Raman spectra, specifically an increase in intensity close to $\sim 160 \text{ cm}^{-1}$. The narrow peak at 170 cm^{-1} for the brominated sample is very sharp (2 cm^{-1}) and should not be related to a RBM feature but to some experimental artifact (such as a plasma line), because the linewidth is less than what is normally observed for a RBM feature (6 – 10 cm^{-1}) in this nanotube diameter range. For the pristine sample, a similar very narrow peak was observed at the same frequency. The changes in the relative RBM intensity of the tubes (9,4), (10,2), and (11,0) after bromination are due to the shift of the electronic transition after doping [see Fig.

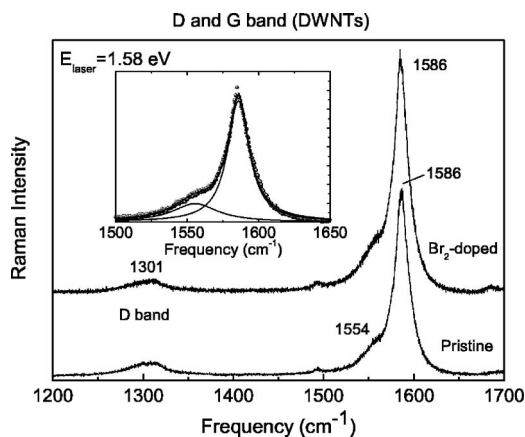


FIG. 6. Raman spectra taken with $E_{\text{laser}}=1.58$ eV for pristine and Br₂-adsorbed DWNTs in the region of the *G* band. The inset shows the line shape analysis for the pristine sample.

2(b)]. Before Br₂ doping, the (11,0) peak has the maximum intensity and the intensity of the (9,4) and (10,2) tubes are weaker. However, upon doping with bromine the RBM intensity for the (9,4) tube decreases because the doping brings the E_{22}^S value further from E_{laser} , while for the (10,2) and (11,0) tubes, the upshift of E_{22}^S leads to more favorable resonance conditions for these tubes, thus leading to an increase in the overall intensity of the Raman RBM feature upon bromination (see Fig. 5). The observation that, within the experimental error, the RBM frequencies for the inner semiconducting tubes do not change after the bromination process indicates that semiconducting inner nanotubes when shielded by metallic outer tubes are not very sensitive to charge transfer effects due to Br₂ doping. In the M/S configuration, the charge transfer should occur predominantly between the bromine and the outer metallic tubes which give electrons to the nearby bromine molecules.

C. *G*-band analysis

The RBM characteristics are more appropriate for analyzing the changes in the electronic transition energies E_{ii} and also for identifying the (n, m) indices of the tubes that are in resonance with a particular E_{laser} . However, the higher frequency modes (the so-called *G* band) are more appropriate for studying charge transfer effects, because the *G* band Raman frequencies are strongly dependent on doping effects, as is also known from graphite intercalation compounds.¹⁴

We start our discussion of the *G* band by analyzing the simplest profile we observed for the *G* band, and this one (see Fig. 6) was taken for $E_{\text{laser}}=1.58$ eV. This profile is typical of semiconducting nanotubes because of its line shape, and is strongly influenced by the small diameter inner semiconducting tubes because the splitting between the upper *G*-band peak (ω_G^+) and the lower *G*-band peak (ω_G^-) is large ($1586-1554=32$ cm⁻¹). This splitting is in agreement with the diameter dependence of these modes that was previously reported.²⁵ We thus conclude that the spectrum in Fig. 6 is dominated by the inner semiconducting tubes. The corresponding splitting for metallic tubes would be about

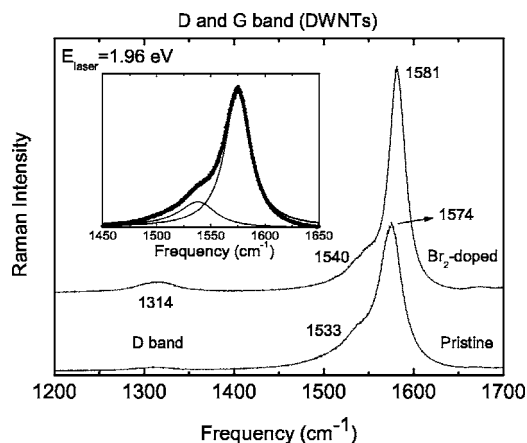


FIG. 7. Raman spectra taken with $E_{\text{laser}}=1.96$ eV for pristine and Br₂-adsorbed DWNTs in the region of the *G* band. The inset shows the line shape analysis for the pristine sample.

twice as large as the observed splitting for semiconducting tubes. It is interesting to note that we do not observe any appreciable shift in the Raman frequencies after Br₂ doping. We attribute the absence of shifts in the *G* band at $E_{\text{laser}}=1.58$ eV to the shielding of the semiconducting inner tubes by the outer metallic tubes. This observation implies a very weak interaction of the inner tubes with the dopant and a small charge transfer effect to the inner semiconducting tubes. Further evidence for the low charge transfer effect from these inner tubes is that the linewidths (18 cm⁻¹ for the G^+ peak and 30 cm⁻¹ for the G^- peak) do not change after Br₂ doping. Therefore, the contribution to the line shape profile from the inner semiconducting tubes should prevail due to the strong resonance condition. No shifts in either ω_{G^-} or ω_{G^+} are observed experimentally. The narrow peak close to 1500 cm⁻¹ that is observed for both the pristine and Br₂-doped samples is identified as an experimental artifact.

The Raman intensity depends sensitively on the electron-phonon coupling that is strongly dependent of the nanotube geometric structure.²² The *G*-band intensity for metallic tubes is generally weaker than for semiconducting tubes, and the overall Raman intensity is also expected to be weaker for tubes with a large diameter, consistent with experimental observation that the outer metallic tubes do not contribute strongly to the *G*-band feature.

The *G*-band spectra obtained with $E_{\text{laser}}=1.96$ eV are shown in Fig. 7. From the analysis of the RBM we know that for this laser energy mainly the inner tubes are in resonance with the incident photons. For this photon energy, the resonant inner tubes are predominantly metallic tubes with a few small diameter semiconducting tubes also contributing to the spectrum. However, in the resonance Raman process, the resonance with the scattered photons should be considered as well as for the *G*-band spectra. Since the *G* band has an energy of 200 meV, this would imply that those nanotubes with E_{ii} close to $1.96-0.1=1.86$ eV would mainly contribute to the *G*-band spectra. By analyzing the Kataura plot in Fig. 2, we can conclude that the *G* band would have contributions from other (n, m) tubes in addition to, rather than only those observed and identified in the RBM spectra of Fig. 4. How-

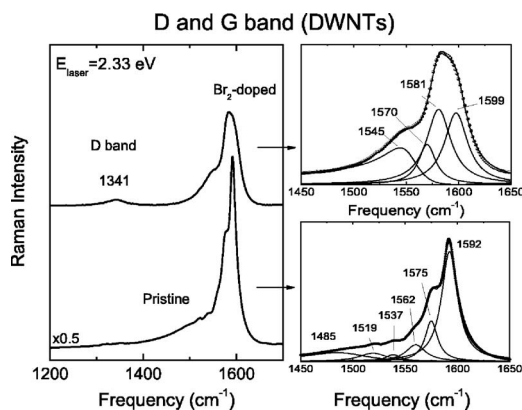


FIG. 8. Raman spectra shown in the left panel are taken with $E_{\text{laser}}=2.33$ eV for pristine and Br_2 -adsorbed DWNTs in the region of the G band. The figures on the right show the line shape analysis for the pristine (lower panel) and the doped (upper panel) samples.

ever, the tubes resonant with the scattered photons are also inner tubes and the main contribution in Fig. 7 comes from the metallic inner tubes. For the spectra taken with 1.96 eV in Br_2 -doped DWNTs, the G band upshifts in frequency by 7 cm^{-1} as compared to pristine samples. This result indicates that there is a depletion in the occupation of electron states from the nanotube valence bands as the Fermi is lowered due to the presence of acceptor Br_2 molecules. Furthermore, the G band of the pristine sample excited with $E_{\text{laser}}=1.96$ eV clearly exhibits a strong Breit-Wigner-Fano line shape for the G -band feature, thus showing that the inner metallic tubes are contributing strongly to the G -band profile. This statement is further supported by checking the observed splitting of the G band as reported in Ref. 25. We can observe in the upper trace of Fig. 7 that the BWF profile is considerably weakened for the Br_2 -adsorbed DWNTs, thus showing that the bromine molecules are removing electrons from the tubes and lowering the Fermi level of the metallic nanotubes, consistent with the upshift of the ω_{G^+} . This conclusion is based on the $I_{\text{BWF}}/(I_{\text{BWF}}+I_G^+)$ intensity ratio obtained by line shape analysis of both the pristine (intensity ratio of 0.35 shown in the inset to Fig. 7) and Br_2 -doped (intensity ratio of 0.20) samples. Furthermore, the G -band linewidths for the pristine sample are approximately 8 cm^{-1} larger than those for the brominated samples probed with 1.58 eV, which is consistent with the fact that metallic nanotubes exhibit a somewhat larger linewidth than semiconducting tubes.²⁵ Upon doping, the G -band intensity increases, thus indicating that a better resonance condition is achieved after doping, in agreement with the RBM analysis. The small increase in the intensity of the D band (the so-called disorder-induced mode) for the Br_2 -adsorbed samples also indicates that some interaction between the acceptor molecules and the outer tubes is occurring. Since the RBM and G -band intensities are not decreased, we conclude that the lowering of the Fermi energy E_F by the charge transfer process is relatively small, and E_F remains above the van Hove singularities of the valence band levels involved in the relevant E_{ij} transitions.

In the left panel of Fig. 8 we show the Raman spectra of the G band for both pristine (lower trace) and Br_2 -doped (upper trace) DWNTs for $E_{\text{laser}}=2.33$ eV. The G band for

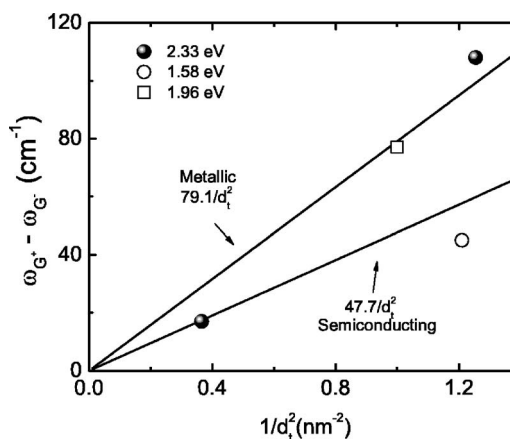


FIG. 9. Dependence of the $\omega_{G^+}-\omega_{G^-}$ splitting on reciprocal diameter. The solid lines come from the dependence of the splitting of SWNTs on $1/d_t^2$ found in Ref. 25 and the points are our experimental data obtained from Figs. 6–8.

pristine DWNTs excited with 2.33 eV (Fig. 8) is special as compared to the 1.58 and 1.96 eV insofar as we can clearly identify the contributions from both the inner and outer tubes in the G -band spectra because they are both in resonance with $E_{\text{laser}}=2.33$ eV, as shown by the RBM spectra. The G -band line shape for the pristine sample is complex, showing many features. In order to better identify the contributions from the inner and outer tubes to the observed profile, we performed the line shape analysis, shown in the right panels of Fig. 8. The strongest mode at 1592 cm^{-1} for the pristine sample has contributions from both the inner and outer tubes. The other modes are identified by examining the $\omega_{G^+}-\omega_{G^-}$ splitting which exhibits a diameter dependence of $1/d_t^2$ that has a different coefficient for metallic and semiconducting nanotubes.²⁶ By determining the average diameter for both the inner and outer tubes observed in the RBM spectra, we can identify whether the peak is due to the outer or inner tube, as shown in Fig. 9 (solid circles). The peak observed at 1575 cm^{-1} in Fig. 8 for the pristine sample is the G^- feature associated with semiconducting nanotubes. We can observe that for the pristine sample there is also a weak BWF tail. This BWF tail in the Raman line shape is typical of metallic tubes interacting with their environment and for our samples the tail originates from the inner tubes that are metallic (see Fig. 2). The $\omega_{G^+}-\omega_{G^-}$ splitting of 108 cm^{-1} is consistent with the expected diameter dependence, as we can see in Fig. 9. Since the inner tubes interact only weakly with the outer tubes which are predominantly semiconducting,¹⁰ it is expected that the BWF contribution to the G -band profile will be relatively weak, in agreement with our experimental observation. The weak G -band peaks at 1519 and 1537 cm^{-1} are due to the E_2 and E_1 symmetry modes, respectively. For completeness sake, we also plot in Fig. 9 the splitting observed for the 1.58 eV (open circle) and 1.96 eV (open square) laser excitation energies, thus confirming our identification that the G -band profile is dominated by semiconducting and metallic nanotubes, respectively.

The G band exhibits significant changes in frequency and intensity after Br_2 doping. By performing a line shape analysis, we can get the changes in the G -band line shape in detail,

as shown on the right-hand panels of Fig. 8. A clear broadening of the *G* band by Br₂ doping is observed at $E_{\text{laser}}=2.33$ eV and this is because the metallic inner and semiconducting outer tubes experience different frequency shifts because of different amounts of charge transfer. The linewidths of the individual lines do not change appreciably after bromination. Metallic and semiconducting tubes both have a G^+ peak at about 1592 cm^{-1} so they sum up to give a strong peak at this frequency for the pristine sample. For Br₂ doped DWNTs, we can observe a G^+ mode at 1599 cm^{-1} that is upshifted by 7 cm^{-1} relative to the 1592 cm^{-1} for the pristine DWNTs. This component is attributed to the outer tubes. We should point out that this upshift is about the same as is observed for the 1.96 eV spectra for metallic inner tubes. Based on the results from electrochemical studies,²⁷ it has been determined that the *G*-band frequency upshift for bromine-doped DWNTs is $326\text{ cm}^{-1}/\text{electron}/\text{carbon atom}$. Thus, the 7 cm^{-1} upshift would imply a charge transfer of 0.02 holes/carbon. The other *G* band components are somewhat more difficult to analyze because of the strong overlap in the contributions from the inner and outer tubes. However, before bromine intercalation, the BWF peak due to the metallic inner tube is clearly identified and it does not overlap with the modes of the outer semiconducting tubes because of the very different diameter dependence of this mode frequency.²⁵ We note that the BWF profile for the inner tube is strongly affected by the Br₂ adsorption. Its frequency exhibits an upshift from 1485 cm^{-1} up to 1545 cm^{-1} . This shows that metallic tubes are very sensitive to doping even though they are here shielded by the outer semiconducting tubes. A similar effect has been observed for iodine-doped DWNTs.¹³ The effect of charge transfer on the electronic transition energies is small for large diameter tubes. Therefore, the intensity of the Raman spectra for the large diameter outer tubes is expected not to vary so much, which is in agreement with the results shown in Figs. 3(a) and 3(b). Therefore, the upshifts due to charge transfer are about the same for both spectra measured with 2.33 and 1.96 eV . For both laser excitation energies, the resonant inner tubes are metallic and the outer tubes are semiconducting, thus showing that the physics behind the charge transfer phenomena is similar, although different (n, m) nanotubes are in resonance at the two laser excitation energies.

Finally we comment on the *D* band intensity for the different laser energies. We observe that the *D* band is essentially absent for the pristine DWNTs and is very weak for the Br₂-adsorbed DWNTs for $E_{\text{laser}}=2.33\text{ eV}$. This result indicates that our samples have a high degree of crystallinity. This observation also indicates that Br₂ molecules do not intercalate in the space between the inner and the outer tubes. The presence of Br₂ in this region would locally deform the nanotube structure, breaking the translational symmetry, which in turn would enhance the *D*-band intensity. The fact that the *D* band is more intense for 1.58 eV than for 2.33 eV laser excitation does not indicate that the tubes probed by the 1.58 eV have more defects than those probed by 2.33 eV . This difference in intensity is due to the laser excitation energy dependence of the *D*-band intensity, in general, and is not specific to the particular sample used in the present study.²⁸ More detailed studies using many laser lines are ex-

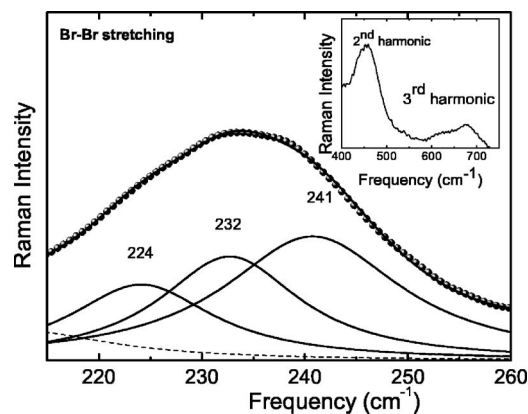


FIG. 10. The line shape analysis for the Raman peaks from the Br₂ intercalant species from the Raman spectrum taken at $E_{\text{laser}}=2.33\text{ eV}$. The dashed line is the contribution from the nanotubes close to 200 cm^{-1} . The inset shows the second and third harmonic modes of the Br-Br stretching mode.

pected to further clarify the observed effects.

D. The vibrational properties of the dopant

Br₂-adsorbed DWNTs are of special interest because we can also observe the Raman spectra of the Br₂ species for the $E_{\text{laser}}=2.33\text{ eV}$ excitation (see Fig. 10). The Br-Br stretching bands for the bromine adsorbed DWNTs are centered at about 233 cm^{-1} . We should point out that this band exhibits a large downshift when compared with solid bromine (300 cm^{-1}) and gaseous Br₂ (324 cm^{-1}).²⁹ For graphite intercalation compounds, the bromine stretching mode was observed at 242 cm^{-1} at a temperature of 77 K . The downshift from 242 to 233 cm^{-1} may be attributed to a hardening of the atomic vibrations due to a decrease in temperature.¹⁴ Of special interest are the Raman spectra of Br₂ doped SWNTs (Ref. 5) taken with $E_{\text{laser}}=2.41\text{ eV}$ which showed sharp peaks characteristic of free Br₂ and a broad band at about 260 cm^{-1} , that was attributed to an upshift by 74 cm^{-1} of the RBM due to charge transfer. Our study suggests that this broad band with a doublet structure may in part be associated with the Br₂ molecules which are adsorbed on the SWNTs and our interpretation of these data would give rise to a downshift of 67 cm^{-1} for their Br-Br stretching mode.

The Br-Br stretching mode in Fig. 10 exhibits a large linewidth (about 33 cm^{-1}) in DWNTs and this linewidth can be attributed to an inhomogeneous environment (different diameters and chiralities and configurations). We therefore analyzed this broad line by decomposing it into three Lorentzian curves, as shown in Fig. 10. We attribute the downshift in frequency to the electron charge transfer to the molecule from the DWNTs. This process changes (renormalizes) the wave functions for the molecular system which in turn also affects the vibrational spectra. One scenario would be to attribute the three peaks to a different interaction of Br₂ with the configurations S/M, M/S, and S/S, due to their respective different carrier densities at room temperature. A broad profile is also found in the Raman spectra reported for Br₂ doped SWNTs.⁵ It should be noted that the 17 cm^{-1} splitting

of the components in Fig. 10 is roughly of the same magnitude as the splitting that appears in the spectra for SWNTs in Ref. 5 at nearly the same E_{laser} value. We should comment that additional broadening observed in the Br-Br stretching modes is attributed to the isotopic effects. The isotopes ^{79}Br and ^{81}Br have the same abundance. Thus three kinds of Br-Br bonds are expected in the Br_2 system. The different masses will give a splitting in frequency of 3 cm^{-1} . Thus, the three peaks observed in the line shape analysis should be attributed to the different outer/inner tube configurations rather than to isotopic effects.

We also observed the second and third harmonics of the Br-Br stretching mode at 454 and 677 cm^{-1} , respectively (see inset to Fig. 10). The observation of harmonics with considerable intensity suggests that a resonance process is occurring for energies close to $E_{\text{laser}}=2.33\text{ eV}$. This statement is also based on the fact that we could not observe the Br_2 Raman spectra for the other two laser lines used in the present study. A more detailed study of the Br-Br stretching mode and its resonance profile is now in progress.

E. Comparison with previous studies on Br_2 -doped nanotube systems

The relatively small upshifts we observed in the G band upon Br_2 doping differs from previous observations on DWNTs.² The 16 cm^{-1} upshift observed by Chen *et al.*² for Br_2 is much larger than what we have observed here for the 2.33 and 1.96 eV excitation energies. These apparent inconsistencies could be related to the specific sample properties, the different sample preparation techniques that were used, and the different amount of Br_2 that was intercalation. Chen *et al.*² used DWNT samples which had a much higher adsorbed Br content because the sample was in equilibrium with Br_2 gas, and in addition the samples in Ref. 2 were prepared via a peapod conversion route, while our DWNTs samples were prepared by a direct process. The strong upshifts they observed in the G band frequency could be either related to a much larger shift in E_F due to charge transfer or to a different ratio of M/S, S/M, and S/S tubes, or it could be related to the intercalation within the SWNT constituent present in their samples or to bromine interaction with the defects in the outer shells of their DWNTs. The presence of defects in the outer walls may allow the Br_2 molecules to interact more strongly with the inner tube of the DWNT. The DWNT samples previously prepared from peapods likely contain more SWNT constituents than our samples.⁴ It has also been shown that Br_2 doping has a stronger effect on SWNTs than on DWNTs.⁵ As we stated before, our samples are of very high quality concerning the very small SWNT admixture, as confirmed by both HRTEM and Raman spectra.⁴ Even after being subjected to high temperature heat treatment, our DWNT samples show only a very small D -band intensity (see Sec. III C), thus indicating almost an absence of structural defects in the tube walls.

The intensity depression in the G -band intensity by a factor of 2 in the spectrum recorded with 2.33 eV excitation is due to the depletion of valence states of the outer tubes. The outer tubes are closer to the bromine molecules and the

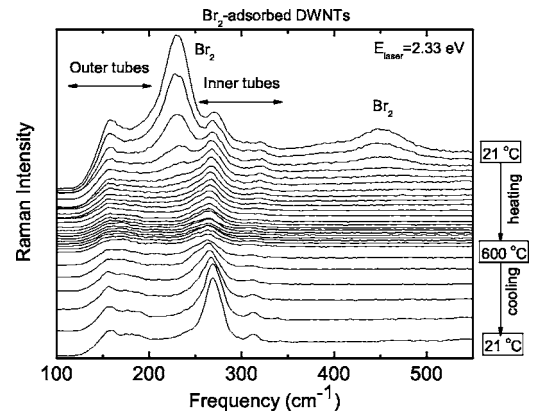


FIG. 11. *In situ* Raman spectra of Br_2 -adsorbed DWNTs subjected to different thermal annealing temperatures during heating (in steps of $25\text{ }^\circ\text{C}$) and cooling (in steps of $100\text{ }^\circ\text{C}$). The Raman spectra were excited by $E_{\text{laser}}=2.33\text{ eV}$.

charge transfer should affect the outer tubes more than the inner tubes. Our experimental observation seems to be in agreement with the previous modeling where about 90% of the charge transfer in DWNTs was found to occur with the outer tubes.² Since, our bromine doping level is not high, the depletion of valence states due to bromination is not large enough to produce a reduction by a factor 40 of the G -band intensity, as previously reported by Chen *et al.*²

The frequency changes observed after doping in carbon nanotubes as a function of doping level are not as clear as in graphite intercalation compounds.¹⁴ Recent studies showed that for both isolated and bundled SWNTs, there is an anomalous change in the C-C bond length upon doping with alkali metals.^{30,31} These metals behave as electron donors and four regimes have been identified in the behavior of the Raman frequencies of SWNT modes as a function of doping concentration.³² For low dopant content, the intercalant adsorption mainly occurs on the outside surface of the bundle and the frequencies do not change. In the second regime of dopant concentration, the G -band frequencies increase and the RBM intensity is suppressed. In the third regime, the frequency of the G band decreases with a continuous loss in intensity. Finally, in regime IV, the G -band frequency remains constant, thus indicating the saturation regime. These results are different from GICs and this difference in behavior should be related to curvature effects in nanotubes. Our observation of upshifts in the G -band modes, suggest that we are in the third regime where the G -band behavior for both donors and acceptors follow what has been established for graphite intercalation compounds. However, in order to check precisely which regime we have in our samples, experiments with different concentrations of Br_2 are needed.

F. Debromination experiments

In order to evaluate how the Br_2 molecules are interacting with our DWNTs, we performed heat treatment experiments on our Br_2 -adsorbed DWNTs. *In situ* temperature-dependent Raman spectra of our brominated DWNTs are shown in Fig. 11. Upon heating, we can observe that the mode at 233 cm^{-1}

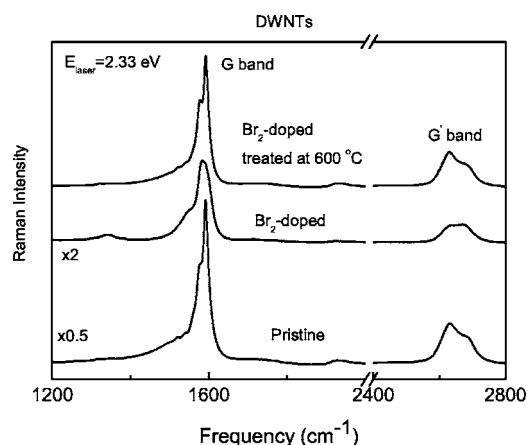


FIG. 12. G-band and G'-band spectra of pristine, Br₂-adsorbed, and thermally treated (600 °C) Br₂-adsorbed DWNTs. The Raman spectra were excited by $E_{\text{laser}}=2.33$ eV.

and its overtone at 460 cm^{-1} , assigned to the Br₂ molecular vibrations, gradually lose intensity, disappearing completely at an annealing temperature of 225 °C. After cooling down to room temperature, we can observe that the RBM spectrum for our samples exhibits slight changes for the outer tubes. The modes close to 270 cm^{-1} are slightly enhanced compared with the Br₂-adsorbed starting sample at room temperature. This could be due to some oxidation effect introduced by the high temperature treatment, which is expected to affect the outer tubes more than the inner tubes, because the inner tubes are shielded by the outer tubes. After cooling the annealed Br₂ adsorbed sample down to 21 °C, the ω_{RBM} is not shifted compared with the pristine samples.

In Fig. 12 we show the high frequency modes of Br₂-adsorbed DWNTs cut after exposure to 600 °C heat treatment temperatures (corresponding to the lowest trace in Fig. 11) and the spectrum for the pristine DWNTs before exposure to Br₂. It is clear that the debromination process is completely reversible, thus indicating a weak interaction between the Br₂ molecules and the DWNTs. A comparison between these spectra also indicates that Br₂ molecules do not intercalate between the inner and outer shells of the DWNTs. The energy needed for removing the Br₂ molecule is around 25 meV (a 200 °C increase in temperature above the ambient of 21 °C). Such a small energy is typical of the physisorption regime. The absence of D-band intensity indicates that for the hydrothermally treated sample, all the Br₂ has been removed and that the doping and undoping processes have not changed the tube structure.

IV. CONCLUSIONS

In summary, we have reported a resonant Raman scattering study of Br₂-adsorbed DWNTs. Spectra are observed for

both the Br-Br molecular vibration, as modified by the intercalation, and the DWNTs vibrations that were observed after intercalation by bromine. The analysis of the resonant Raman profiles associated with the DWNTs allowed us to identify the (n, m) tubes that were contributing to the RBM spectra and how the electronic transition energies for the tubes were affected by the Br₂ doping. By making measurements at $E_{\text{laser}}=2.33, 1.96,$ and 1.58 eV we can probe S/M, M/S, and S/S outer/inner tubes under different bromine intercalation regimes. This allowed us to monitor different charge transfer characteristics to the inner and outer tubes from the adsorbed bromine in these different structural configurations. The analysis of the Raman spectra show that the Br₂ molecules decorate the outer tube surface of the individual DWNT tubes and the spectra further show that the adsorbed bromine molecules behave as an electron acceptor. We have also shown that the Br₂ adsorption in DWNTs is completely reversible upon thermal annealing to 600 °C. Furthermore, we observe that metallic tubes are extremely sensitive to doping and the presence of Br₂ molecules affect their Raman spectra even when the metallic nanotubes are the inner tubes of the DWNTs.

The present work contributes to further understanding the doping effects in DWNTs because we have been able to study the effect of doping on the vibrational properties of selected $2n+m$ families for the inner tubes. In addition, we reported the observation of Raman lines due to the resonance with the upper electronic transition energy $E_{11}^{\text{M}}(\text{H})$ for metallic tubes. A detailed study of the various new phenomena reported here would require the use of tunable lasers and doped samples with different amounts of dopant and charge transfer. Such studies would allow us to separate the contributions of the doping to the Fermi energy shift from the shifting in the electronic transition energies as bromine intercalation takes place.

ACKNOWLEDGMENTS

A.G.S.F. acknowledges FUNCAP (Grant No. PPP-985/03) and CNPq (Grant Nos. 307417/2004-2 and 55.6549/2005-8) Brazilian agencies for partial support and the JST-Japan for supporting the visit to Tohoku University. A.G.S.F. also acknowledges support from Instituto de Nanotecnologia e Rede Nacional de Pesquisa em Nanotubos de Carbono. The MIT authors acknowledge financial support from the NSF (Grant No. DMR04-05538). R.S. acknowledges a Grant-in-Aid (No. 16076201) from MEXT, Japan. The Shinshu University authors acknowledge the CLUSTER of Ministry of Education, Culture, Sports, Science and Technology in Japan for financial support.

*Electronic address: agsf@fisica.ufc.br

- ¹M. Endo, T. Hayashi, H. Muramatsu, Y.-A. Kim, H. Terrones, M. Terrones, and M. S. Dresselhaus, *Nano Lett.* **4**, 1451 (2004).
- ²G. Chen, S. Bandow, E. R. Margine, C. Nisoli, A. N. Kolmogorov, V. H. Crespi, R. Gupta, G. U. Sumanasekera, and P. C. Eklund, *Phys. Rev. Lett.* **90**, 257403 (2003).
- ³S. B. Legoas, V. R. Coluci, S. F. Braga, P. Z. Coura, S. O. Dantas, and D. S. Galvao, *Phys. Rev. Lett.* **90**, 055504 (2003).
- ⁴M. Endo, H. Muramatsu, T. Hayashi, Y. A. Kim, M. Terrones, and M. S. Dresselhaus, *Nature (London)* **433**, 476 (2005).
- ⁵A. M. Rao, P. C. Eklund, S. Bandow, A. Thess, and R. E. Smalley, *Nature (London)* **388**, 257 (1997).
- ⁶S. Bandow, G. Chen, G. U. Sumanasekera, R. Gupta, M. Yudasaka, S. Iijima, and P. C. Eklund, *Phys. Rev. B* **66**, 075416 (2002).
- ⁷P. Corio, A. P. Santos, M. L. A. Temperini, V. W. Brar, M. A. Pimenta, and M. S. Dresselhaus, *Chem. Phys. Lett.* **383**, 475 (2004).
- ⁸X. Liu, T. Pichler, M. Knupfer, J. Fink, and H. Kataura, *Phys. Rev. B* **70**, 205405 (2004).
- ⁹S. B. Fagan, A. G. S. Filho, J. M. Filho, P. Corio, and M. S. Dresselhaus, *Chem. Phys. Lett.* **456**, 54 (2005).
- ¹⁰R. Pfeiffer, F. Simon, H. Kuzmany, and V. N. Popov, *Phys. Rev. B* **72**, 161404(R) (2005).
- ¹¹L. Duclaux, *Carbon* **1751**, 717 (2002).
- ¹²J. E. Fischer, *Acc. Chem. Res.* **35**, 1079 (2002).
- ¹³J. Cambedouzou, J. L. Sauvajol, A. Rahmani, E. Flahaut, A. Peigney, and C. Laurent, *Phys. Rev. B* **69**, 235422 (2004).
- ¹⁴M. S. Dresselhaus and G. Dresselhaus, *Adv. Phys.* **30**, 139 (1981).
- ¹⁵H. Son, A. Reina Cecco, Ge. G. Samsonidze, R. Saito, A. Jorio, J. Kong, and M. S. Dresselhaus (unpublished).
- ¹⁶A. Jorio, C. Fantini, M. A. Pimenta, R. B. Capaz, G. G. Samsonidze, G. Dresselhaus, M. S. Dresselhaus, J. Jiang, N. Kobayashi, A. Grüneis, and R. Saito, *Phys. Rev. B* **71**, 075401 (2005).
- ¹⁷V. N. Popov, *New J. Phys.* **6**, 17 (2004).
- ¹⁸Ge. G. Samsonidze, R. Saito, N. Kobayashi, A. Grüneis, J. Jiang, A. Jorio, S. G. Chou, G. Dresselhaus, and M. S. Dresselhaus, *Appl. Phys. Lett.* **85**, 5703 (2004).
- ¹⁹P. G. Collins, M. S. Arnold, and P. Avouris, *Science* **292**, 706 (2001).
- ²⁰R. Saito, G. Dresselhaus, and M. S. Dresselhaus, *Phys. Rev. B* **61**, 2981 (2000).
- ²¹Ge. G. Samsonidze, R. Saito, J. Jiang, A. Grüneis, N. Kobayashi, A. Jorio, S. G. Chou, G. Dresselhaus, and M. S. Dresselhaus, "Corrections to the optical transition energies in single-wall carbon nanotubes of smaller diameters," in *Functional Carbon Nanotubes: MRS Symposium Proceedings, Boston, December 2004*, edited by D. L. Carroll, B. Weisman, S. Roth, and A. Rubio (Materials Research Society, Warrendale, PA, 2005).
- ²²J. Jiang, R. Saito, Ge. G. Samsonidze, S. G. Chou, A. Jorio, G. Dresselhaus, and M. S. Dresselhaus, *Phys. Rev. B* **72**, 235408 (2005).
- ²³J. Jiang, R. Saito, A. Grüneis, G. Dresselhaus, and M. S. Dresselhaus, *Carbon* **42**, 3169 (2004).
- ²⁴C. Fantini, A. Jorio, M. Souza, M. S. Strano, M. S. Dresselhaus, and M. A. Pimenta, *Phys. Rev. Lett.* **93**, 147406 (2004).
- ²⁵A. Jorio, C. Fantini, M. S. S. Dantas, M. A. Pimenta, A. G. SouzaFilho, G. G. Samsonidze, V. W. Brar, G. Dresselhaus, M. S. Dresselhaus, A. K. Swan, M. S. Ünli, B. B. Goldberg, and R. Saito, *Phys. Rev. B* **66**, 115411 (2002).
- ²⁶A. Jorio, A. G. Souza Filho, G. Dresselhaus, M. S. Dresselhaus, A. K. Swan, M. S. Ünli, B. B. Goldberg, M. A. Pimenta, J. H. Hafner, C. M. Lieber, and R. Saito, *Phys. Rev. B* **65**, 155412 (2002).
- ²⁷P. Chen, X. Wu, J. Lin, and K. Tan, *Science* **285**, 91 (1999).
- ²⁸K. Sato, R. Saito, Y. Oyama, J. Jiang, L. G. Cancado, M. A. Pimenta, A. Jorio, Ge. G. Samsonidze, G. Dresselhaus, and M. S. Dresselhaus, *Chem. Phys. Lett.* (to be published).
- ²⁹J. E. Cahill and G. E. Leroi, *J. Chem. Phys.* **51**, 4514 (1969).
- ³⁰G. Chen, C. A. Furtado, U. J. Kim, and P. C. Eklund, *Phys. Rev. B* **72**, 155406 (2005).
- ³¹G. Chen, C. A. Furtado, S. Bandow, S. Iijima, and P. C. Eklund, *Phys. Rev. B* **71**, 045408 (2005).
- ³²A. Kim *et al.* (unpublished).